

ORIGINAL ARTICLE

# Sphingomyelin-induced inhibition of the plasma membrane calcium ATPase causes neurodegeneration in type A Niemann–Pick disease

A Pérez-Cañamás<sup>1</sup>, S Benvegnù<sup>1</sup>, CB Rueda<sup>1,2,3</sup>, A Rábano<sup>4</sup>, J Satrústegui<sup>1,2,3</sup> and MD Ledesma<sup>1</sup>

Niemann–Pick disease type A (NPA) is a rare lysosomal storage disorder characterized by severe neurological alterations that leads to death in childhood. Loss-of-function mutations in the acid sphingomyelinase (ASM) gene cause NPA, and result in the accumulation of sphingomyelin (SM) in lysosomes and plasma membrane of neurons. Using ASM knockout (ASMko) mice as a NPA disease model, we investigated how high SM levels contribute to neural pathology in NPA. We found high levels of oxidative stress both in neurons from these mice and a NPA patient. Impaired activity of the plasma membrane calcium ATPase (PMCA) increases intracellular calcium. SM induces PMCA decreased activity, which causes oxidative stress. Incubating ASMko-cultured neurons in the histone deacetylase inhibitor, SAHA, restores PMCA activity and calcium homeostasis and, consequently, reduces the increased levels of oxidative stress. No recovery occurs when PMCA activity is pharmacologically impaired or genetically inhibited *in vitro*. Oral administration of SAHA prevents oxidative stress and neurodegeneration, and improves behavioral performance in ASMko mice. These results demonstrate a critical role for plasma membrane SM in neuronal calcium regulation. Thus, we identify changes in PMCA-triggered calcium homeostasis as an upstream mediator for NPA pathology. These findings can stimulate new approaches for pharmacological remediation in a disease with no current clinical treatments.

*Molecular Psychiatry* advance online publication, 13 September 2016; doi:10.1038/mp.2016.148

## INTRODUCTION

Niemann–Pick disease includes various genetic mutations in metabolism yielding three discernable subtypes.<sup>1,2</sup> Niemann–Pick patients suffering from types A (NPA) and B (NPB) carry mutations in the acid sphingomyelinase (ASM) gene that reduce the activity of this enzyme to different extent.<sup>3</sup> Both types share hepatosplenomegaly and lung pathology. However, severe neurological alterations leading to death in early childhood only occur in NPA patients, whereas NPB patients present with little to no neurological involvement and frequently live into adulthood. Niemann–Pick type C (NPC) patients carry mutations in the genes encoding for the cholesterol transport proteins Npc1 or Npc2 and may have mild hepatosplenomegaly but profound alterations in the central nervous system functioning.<sup>1</sup> The small iminosugar, Miglustat, which inhibits glycosphingolipid synthesis, has efficacy to improve or stabilize clinical markers in NPC.<sup>4</sup> Intravenous infusion of recombinant ASM improves disease symptoms in NPB patients.<sup>5</sup> However, no treatment is currently available for NPA.

ASM mutations specifically leading to NPA reduce ASM activity to < 1% of its normal capacity.<sup>3</sup> ASM degrades sphingomyelin (SM) in lysosomes,<sup>6</sup> and its deficiency induces the accumulation of SM and its derivatives in these organelles. So, NPA is considered a lysosomal storage disorder (LSD)<sup>7</sup> that involves lysosomal membrane permeabilization and impaired autophagy.<sup>8</sup> ASM-deficient cells undergo lysosomal exocytosis after wounding but display poor injury-dependent endocytosis and plasma membrane repair.<sup>9</sup> Recent studies in mice that lack ASM (ASMko)<sup>10</sup> indicate that a non-lysosomal component in NPA disease

pathology could account for neural deficits, including cognitive alterations.<sup>11–13</sup> In ASMko mice, excess SM and its derivatives also occur in the plasma and synaptic membranes of hippocampal neurons, which cause abnormal axonal membrane polarization,<sup>14</sup> deficient synaptic vesicle docking<sup>15</sup> and dendritic spine anomalies.<sup>12</sup>

We hypothesize that oxidative stress and a loss of calcium homeostasis are common features that underlie the pathology of different LSDs,<sup>16,17</sup> such as NPA, even though the specific underlying mechanisms in each LSDs presumably differ. Understanding the mechanisms that promote oxidative stress and altered calcium homeostasis will provide insight into the functional consequences that arise in NPA pathology and other LSDs.

## MATERIALS AND METHODS

### Antibodies

Antibodies against the following proteins or epitopes were used to probe western blots: alpha-tubulin (Abcam, Cambridge, UK, 7291), PMCA (Thermo Fisher Scientific, Waltham, MA, USA, MA3-914), vinculin (Merck Millipore, Darmstadt, Germany, AB6039), GAPDH (Abcam, ab8245), ATP6V1A (Proteintech, Manchester, UK, 17115-1-AP), Ac-H3K18 and H3 (Cell Signaling, Danvers, MA, USA, 9927), flotillin1 (BD Transduction Laboratories, San Jose, CA, USA, 610821), beta-actin (Sigma-Aldrich, St. Louis, MO, USA, A5441), GFAP (Dako, Glostrup, Denmark, Z0334), MAP2 (Covance, Princeton, NJ, USA, PCK-554P), PMCA2 (Thermo Fisher Scientific, PA1-915) and cleaved caspase-3 (Asp 175) (Cell Signaling, 9661). HRP-conjugated

<sup>1</sup>Centro Biología Molecular Severo Ochoa, CSIC-UAM, Madrid, Spain; <sup>2</sup>Centro de Investigación Biomédica en Red de Enfermedades Raras (CIBERER), Madrid, Spain; <sup>3</sup>Instituto de Investigaciones Sanitarias, Fundación Jiménez Díaz, Madrid, Spain and <sup>4</sup>Fundación Centro de Investigación de Enfermedades Neurológicas (CIEN), Madrid, Spain. Correspondence: Dr MD Ledesma, Centro Biología Molecular Severo Ochoa, Nicolás Cabrera 1, Madrid 28049, Spain.

E-mail: dledesma@cbm.csic.es

Received 1 February 2016; revised 28 June 2016; accepted 13 July 2016

goat anti-rabbit and rabbit anti-mouse antibodies (Dakocytomation, Glostrup, Denmark) were used as secondary antibodies.

### Human samples

Formaldehyde-fixed brain tissue from a 3-year-old NPA patient and a 2-year-old control child was donated by the Wylder Nation Foundation (<http://wyldernation.org/>) and the Fundación Cien brain bank (<http://bt.fundacioncien.es/#>), respectively. Paraffin sections were unstained or stained with either hematoxylin–eosin or antibodies against MAP2 or calbindin D-28k (Swant, Marly, Switzerland, McAB 300) using conventional protocols.

### Mice

A breeding colony was established from ASM heterozygous C57BL/6 mice, kindly donated by Prof. E.H. Schuchman (Mount Sinai School of Medicine, New York, NY, USA). Male wild type (wt) and ASMko littermates were identified by PCR performed on DNA isolated from the tail<sup>10</sup> and then were randomly assigned to experimental groups. All experiments and treatments were conducted blind to the sample group allocation. Internal review boards at the CBMSO and CSIC approved all procedures involving the use of mice performed in accordance with specific European Union guidelines for the protection of animal welfare (Directive 2010/63/EU).

### Treatments in cultured hippocampal neurons

Primary cultures of hippocampal neurons were prepared from wt and ASMko mouse embryos as described previously.<sup>14</sup> Where necessary, SM (Sigma) was added to the medium at a concentration of 40  $\mu\text{M}$ , Apocynin (Calbiochem, Darmstadt, Germany) at 0.5 mM and BAPTA-AM (Invitrogen, Carlsbad, CA, USA) at 10  $\mu\text{M}$  for the times indicated. In some instances, SM was added to the medium 30 min after the addition of the neutral and acid sphingomyelinases inhibitors, GW4869 (15  $\mu\text{M}$ : Cayman Chemical, Ann Arbor, MI, USA) and Siramesine (5  $\mu\text{M}$ : Sigma), respectively.

### SM analysis

Biochemical analysis of SM was performed as described elsewhere,<sup>12</sup> and the determination of SM by lysenin staining<sup>14</sup> was conducted on cultured neurons.

### Lipofuscin and reactive oxygen species determination

Mice were killed by decapitation, and their brain was quickly removed to obtain hippocampal slices (400  $\mu\text{m}$ ). These slices were then equilibrated for 1 h in artificial cerebrospinal fluid (ACSF). To assess reactive oxygen species (ROS), slices or cultured neurons were incubated for 20 min with dihydrorhodamine 123 (10  $\mu\text{M}$ , DHR: Molecular Probes, Carlsbad, CA, USA). The fluorescence product of DHR, rhodamine-123, was detected at excitation and emission wavelengths of 500 and 536 nm, respectively. By contrast, autofluorescence associated with lipofuscin aggregates was detected at excitation and emission wavelengths of 360 and 540–640 nm, respectively. Incubation for 10 min with Sudan black B (10 mg  $\text{ml}^{-1}$ : Santa Cruz, Dallas, TX, USA), which quenches lipofuscin autofluorescence, and granule detection by bright field microscopy confirmed this pigment identity. Images of hippocampal slices were captured on a confocal microscope (LSM510, Zeiss, Oberkochen, Germany) and those of the cultured neurons on an Axiovert200 microscope (Oberkochen, Germany).

### Calcium recordings

For single-cell calcium imaging, hippocampal neurons were seeded at 40 000 cells  $\text{cm}^{-2}$  and maintained in culture for 12 days (12 DIV). The neurons were then loaded for 30 min at 37 °C with Fura2-AM (5  $\mu\text{M}$ : Molecular Probes) and pluronic acid F.127 (50  $\mu\text{M}$ : Invitrogen) in a  $\text{Ca}^{2+}$ -free HCSS buffer (120 mM NaCl, 5.4 mM KCl, 0.8 mM  $\text{MgCl}_2$ , 25 mM HEPES at pH 7.4) containing 2.5 mM glucose. After loading, the cells were washed for 30 min with HCSS containing 2 mM  $\text{CaCl}_2$  and 2.5 mM glucose. Subsequently, the coverslips were mounted in a chamber on the microscope stage, and Fura2-AM fluorescence was imaged ratiometrically at 37 °C using alternate excitation at 340 and 380 nm, and a 510 nm emission filter associated with a Neofluar 40 $\times$ /0.75 objective (Zeiss). KCl (30 mM) was added and a single-cell analysis of the changes in  $[\text{Ca}^{2+}]_i$  was expressed in nM, as deduced from the ratio of fluorescence intensity at 340 ( $F_{340}$ ) and 380 nm ( $F_{380}$ ;  $F_{340}/F_{380}$ ).<sup>18</sup> Image acquisition and analysis were performed

with Aquacosmos 2.5 software (Hamamatsu Photonics, Hamamatsu, Japan), and the fluorescence ratios were corrected for autofluorescence, which was determined after the addition of digitonin and 4 mM  $\text{MnCl}_2$ . For the superfusion experiments HCSS was used in continuous superfusion ( $\approx 1.5 \text{ ml min}^{-1}$ ). Sequential addition of KCl for 1 min was achieved by replacing 30 mM NaCl with 30 mM KCl in the HCSS buffer, and 120 mM NaCl was replaced with 112.5 mM choline (Merck, Darmstadt, Germany) to block the NCX exchanger. The data from these experiments was represented as an  $F_{340}/F_{380}$  ratio ( $R$ ) with respect to the initial ratio ( $R_0$ ;  $R/R_0$ ).

### Calcium-ATPase activity

The hippocampus was homogenized in a buffer containing 10 mM HEPES/KOH, 0.32 M sucrose, 0.5 mM  $\text{MgSO}_4$ , 2 mM 2-mercaptoethanol and a protease inhibitor cocktail (Roche, Mannheim, Germany) at pH 7.4. The homogenate was centrifuged for 10 min at 1500  $g$ , and the recovered supernatant was centrifuged for an additional 45 min at 100 000  $g$ . The final pellet was resuspended in a 10 mM HEPES/KOH solution (pH 7.4) containing 0.32 M sucrose, and when indicated, membranes were disrupted by adding Saponin (0.01%: Sigma). The activity of each type of  $\text{Ca}^{2+}$ -ATPase in hippocampal membranes (40  $\mu\text{g}$ ) was measured by following the change in NADH absorption spectrophotometrically at 340 nm in a coupled enzyme assay.<sup>19</sup> Membranes were incubated for 4 min at 37 °C in a final volume of 1 ml of the standard assay medium: 50 mM HEPES/KOH (pH 7.4), 100 mM KCl, 2 mM  $\text{MgCl}_2$ , 5 mM  $\text{Na}_2\text{N}$ , 3.16  $\mu\text{M}$  free  $\text{Ca}^{2+}$  (pCa 5.5, adjusted with 100  $\mu\text{M}$  BAPTA: Sigma), 0.42 mM phosphoenolpyruvate (Sigma), 0.22 mM NADH, 10 IU pyruvate kinase, and 28 IU lactate dehydrogenase (Roche). The reaction was started by adding 1 mM ATP (Sigma), and 100 nM thapsigargin to inhibit SERCA activity, 2  $\mu\text{M}$  vanadate to selectively inhibit PMCA activity, and 3 mM EGTA to measure the  $\text{Mg}^{2+}$ -ATPase activity, were then added consecutively. ATP consumption was measured after each addition to evaluate the contribution of each ATPase to total ATPase activity.

### PMCA inhibition with Caloxin 2a1

Caloxin 2a1 (VSNWNWSPSSGGG-NH2), a specific inhibitor of PMCA,<sup>20</sup> was custom-synthesized by the proteomics service of the Centro Biología Molecular Severo Ochoa (CBMSO). ASMko and wt-cultured neurons were incubated with 400  $\mu\text{M}$  Caloxin 2a1 for 1 h.<sup>21</sup>

### PMCA inhibition with lentiviral vectors expressing shRNAs

Packaging plasmids and short hairpin RNA (shRNA) plasmids against PMCA2 or a scrambled control plasmid (pGFP-C-shLenti) were purchased from Origene (Rockville, MD, USA), and lentiviral particles were produced according to the supplier's instructions. Viruses were added to the medium of 7–8 DIV neurons and after overnight infection, this medium was replaced by neuronal conditioned medium.

### Raft isolation

Extracts from 12 DIV hippocampal neurons were incubated for 40 min at 4 °C under rotation in TNE buffer (50 mM Tris–HCl, 150 mM NaCl, 5 mM EDTA (pH 7.4)) containing 1% Triton X-100 and a protease inhibitor cocktail. The suspension was centrifuged at 100 000  $g$  for 1 h at 4 °C. After centrifugation, the detergent-insoluble membranes (raft) were collected from the pellet, whereas detergent soluble material (non-raft) was retrieved from the supernatant.<sup>14</sup>

### PMCA and GM1 co-localization

Cultured neurons (12 DIV: wt, ASMko and SM-treated) were fixed and incubated for 30 min with Alexa-488 conjugated cholera toxin subunit B (1  $\mu\text{g ml}^{-1}$ : Life Technologies, Carlsbad, CA, USA). PMCA was detected by incubation for 1 h with the primary antibody against this protein and subsequently for 1 h with an Alexa-555 conjugated secondary antibody. Images were taken under a confocal microscope (LSM510, Zeiss), subtracting the background using ImageJ software (NIH, <http://imagej.nih.gov/ij/>). The Manders coefficient for PMCA (the fraction of PMCA that co-localizes with GM1) was obtained by applying the threshold IsoData and using the JACoP plugin.

### SAHA treatments

Cultured hippocampal neurons were treated with SAHA (Medchem Express, Monmouth Junction, NJ, USA; dissolved in DMSO) at a final

concentration of 4 and 8  $\mu\text{M}$ . The final DMSO concentration was 0.042% with respect to the culture media. In the experiments aimed to test whether the effects of SAHA on ROS and intracellular calcium levels were PMCA dependent, the levels of the cation were measured in cultured neurons treated with 8  $\mu\text{M}$  SAHA for 2 days and 400  $\mu\text{M}$  Caloxin 2a1 for 1 h or in neurons infected with lentiviral vectors expressing shRNAs and treated 5 days after infection with 8  $\mu\text{M}$  SAHA for two more days.

For *in vivo* treatments, SAHA was solubilized in 5 molar equivalents of HOP- $\beta$ -CDX (Sigma) in water as described previously.<sup>22</sup> SAHA (0.67 g) was added to the solution of HOP- $\beta$ -CDX (18 g in 1 l of water), heated until it dissolved and cooled on ice to room temperature. A solution containing SAHA was administered to 2-month-old mice in the drinking water, and it was replaced weekly. Given that a 20 g mouse drinks approximately 3 ml of water per day, this dosage equals 100 mg of SAHA per kg of body weight per day. Control mice received an equivalent concentration of HOP- $\beta$ -CDX alone, and as an additional control, a group of wt and ASMko mice received only water.

### Memory and motor analysis

The Y-maze was performed as in ref. 23. During the first training trial lasting 8 min, the mice only explored two arms (the initial arm and one other arm), maintaining the third or novel arm closed. After 1 h, the mice were placed in the same starting arm with free access to all three arms for 5 min. The time spent in the novel arm was counted and expressed as a percentage of the total exploration time.

The Rotarod test was performed in an accelerating Rotarod apparatus (Ugo Basile, Varese, Italy), on which the mice were trained for 2 days at a constant speed: the first day—four times at 4 r.p.m. for 1 min and on the second day—four times at 8 r.p.m. for 1 min. On the third day, the Rotarod was set to progressively accelerate from 4 to 40 r.p.m. for 5 min, and the mice were tested four times. During the accelerating trials, the latency to fall from the rod was measured.

### Calbindin and fractin staining

Mice were killed with CO<sub>2</sub> and their cerebellum and hippocampus were dissected, fixed overnight at 4 °C in 4% paraformaldehyde in phosphate-buffered saline and cryoprotected in 30% sucrose in phosphate-buffered saline for 48 h. The tissue was then frozen in Tissue-Tek Optimal Cutting Temperature compound (Sakura Finetek, Torrance, CA, USA), and 30  $\mu\text{m}$  sagittal microtome sections were obtained (CM 1950 Ag Protect freezing; Leica, Solms, Germany). The sections were incubated overnight at 4 °C with the antibodies against calbindin D-28k (Swant, McAB 300) and fractin (Thermo Scientific, P219466) and then with the corresponding Alexa-conjugated secondary antibodies (Invitrogen). Finally, the sections were incubated for 10 min with DAPI (1/5000; Calbiochem), washed and mounted with Prolong Gold Antifade (Invitrogen). Images were obtained on a confocal LSM710 microscope (Carl Zeiss).

### Statistics

The data from at least three different experimental groups was quantified and presented as the mean ( $\pm$  s.e.m.). Normality of the data was tested using the Shapiro–Wilk test. For two-group comparisons, the Mann–Whitney *U*-test for non-parametric data or a two-sample Student's *t*-test for data with parametric distribution were used. For multiple comparisons, data with a normal distribution was analyzed by two-way ANOVA followed by a minimum significant difference or a Games–Howell *post hoc* test. The statistical significance of non-parametric data was determined by the Kruskal–Wallis test to analyze all experimental groups. The Mann–Whitney *U*-test was used to analyze paired genotypes, applying the Bonferroni correction. *P*-values < 0.05 were considered significant, and the statistical tests and sample size (*n* values) used in the experiments are specified in the figure legends. In the figures, asterisks indicate the *P*-values: \* < 0.05; \*\* < 0.005; \*\*\* < 0.001. SPSS 20.0 software (IBM, Armonk, NY, USA) was used for all statistical analyses.

## RESULTS

Neuronal death and oxidative stress in the brain of a NPA patient  
The low prevalence of NPA has limited the number of studies that have characterized neuro-pathological hallmarks in a patient. Immunohistochemical analysis of the brain from a 3-year-old child diagnosed with NPA was conducted using the neuronal marker

MAP2 and Calbindin, a marker of Purkinje cells. This analysis revealed massive neuronal death in all areas analyzed, including the hippocampus, cortex and cerebellum (Supplementary Figures S1a–c). In addition, GFAP staining for astrocytes showed altered morphology, such as decreased cell body size and increased fibers in the hippocampus, and increased cell numbers in the cortex and cerebellum (Supplementary Figures S1d–f). These results indicate that neuronal death and astrogliosis are pathological characteristics of NPA. Furthermore, surviving neurons had enlarged cell bodies containing microgranular refringent deposits (Figure 1b) that were not evident in the brain from a control 2-year-old child (Figure 1a). These deposits autofluoresced intensely indicative of lipofuscin-like aggregates that form due to oxidation and ROS accumulation (Figure 1c). Indeed, lipofuscin granules suggest oxidative stress,<sup>24</sup> which could contribute to the observed large-scale neurodegeneration in NPA.

SM induces increased intracellular calcium levels that promotes oxidative stress in ASMko neurons

We investigated the mechanism by which ASM deficiency stimulates oxidative stress and neuronal death, as observed in the brain of the NPA affected child. So, we examined the hippocampus, an area particularly vulnerable to oxidative stress,<sup>25</sup> in ASMko mice. ASMko mice reproduce NPA human clinical pathology, as mutations in the ASM gene lead to an almost complete loss of enzyme activity. SM levels increase progressively in the brains of ASMko mice, increasing five- to six-fold compared with wt mice at the terminal stage of the disease.<sup>10,14</sup> This increase mimics that reported in the brains of NPA patients.<sup>26</sup> Autofluorescent lipofuscin aggregates were abundant in the hippocampus of ASMko mice by 4 months of age (Figure 1d). Aggregate identity was confirmed by autofluorescence quenching with Sudan black B and bright field microscopy (Supplementary Figure S2). This represents an early disease stage in this animal model, as hippocampal SM levels are only two-fold higher than in wt mice (Supplementary Figure S3a). SM also accumulates in the plasma membrane of hippocampal neurons from ASMko mice in culture as evident by staining with the SM specific probe lysenin (Supplementary Figure S3b).

To determine whether high levels of SM directly cause lipofuscin expression, 12 DIV hippocampal neurons from wt mice were incubated with SM (40  $\mu\text{M}$ ) to increase this lipid content at the plasma membrane (Supplementary Figure S3c). SM accumulation almost doubled (1.8-fold) the number of neurons with lipofuscin aggregates after 48 h (Figure 1e), which was prevented by application of the antioxidant apocynin (0.5 mM; Figure 1e). To directly test the occurrence of oxidative stress in ASMko conditions, we performed DHR staining, which measures ROS levels in living tissue. A two-fold increase in DHR staining was observed in the hippocampus of 4-month-old ASMko compared with wt mice (Figure 1f) and was 1.5-fold higher in 12 DIV ASMko neurons (Figure 1g).

We confirmed the role of SM in ROS accumulation through DHR staining of cultured wt neurons incubated with SM in the presence or absence of antioxidants. Incubation with SM (40  $\mu\text{M}$ ) for 16 h increased the amount of SM to levels found in ASMko neurons (Supplementary Figures S3b and c) and increased ROS levels by 30% (Figure 1h). This effect was prevented by incubation with the antioxidant apocynin (0.5 mM; Figure 1h). To rule out that the increased ROS was due to SM metabolites, we repeated these experiments in the presence of inhibitors of neutral (GW4869) and acid (Siramesine) sphingomyelinases responsible for SM degradation at the plasma membrane.<sup>27,28</sup> The presence of GW4869 (15  $\mu\text{M}$ ) and Siramesine (5  $\mu\text{M}$ ) prevented SM metabolite formation,<sup>28,29</sup> whereas simultaneously increasing plasma membrane SM levels 2.5-fold (Supplementary Figure S3d). However, this treatment did not prevent ROS increases (Figure 1i). These results indicate that high SM levels can induce oxidative stress in ASMko neurons.

Calcium imbalances are a main source of oxidative stress in cells,<sup>30,31</sup> so we assessed whether this imbalance occurs in ASM-deficient neurons by monitoring intracellular calcium in 12 DIV hippocampal neurons from wt and ASMko mice. Calcium

levels were measured by loading neurons with Fura2-AM, a high affinity intracellular calcium indicator.<sup>18</sup> These experiments were performed at steady state conditions and following stimulation by high potassium depolarization (Figures 2a and b). In ASMko

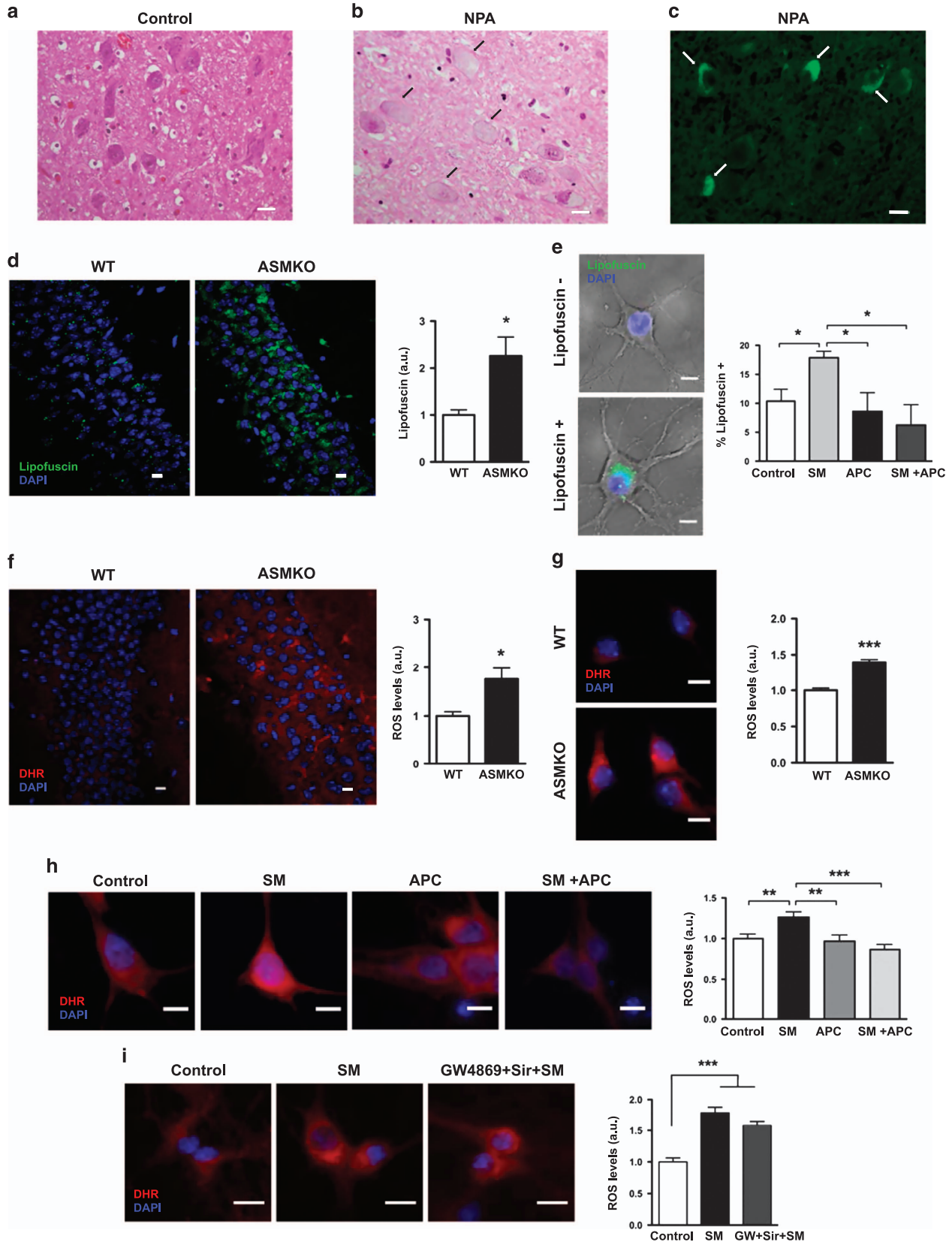


**Figure 1.** High oxidative stress in neurons of a Niemann–Pick disease type A (NPA) affected child, ASM knockout (ASMko) mice and sphingomyelin (SM)-treated wild-type (wt) neurons. **(a,b)** Hematoxylin–eosin staining of the solitary tract nucleus of a control **(a)** and NPA affected **(b)** child. Black arrows indicate microgranular refringent deposits in NPA neurons. **(c)** Fluorescence microscopy image of unstained sections of the solitary tract nucleus in the NPA brain. The white arrows indicate autofluorescent microgranular deposits. Scale bars in **a–c** = 25  $\mu\text{m}$ . **(d)** Lipofuscin aggregates in the hippocampus of 4-month-old wt and ASMko mice. The graph shows the mean ( $\pm$  s.e.m.) lipofuscin fluorescence intensity per area unit ( $n=5$ , Student's *t*-test,  $P=0.047$ ). **(e)** Merged phase contrast and fluorescence images of hippocampal neurons from wt mice with or without lipofuscin inclusions. The graph shows the mean ( $\pm$  s.e.m.) percentage of lipofuscin positive neurons in hippocampal cultures from wt mice when untreated (control), treated with SM (SM), with the antioxidant apocynin (APC) or with SM and apocynin (SM+APC) ( $n=100$  neurons from four cultures, two-way ANOVA followed by minimum significant difference (MSD):  $P_{\text{ctl/sm}}=0.048$ ,  $P_{\text{sm/apc}}=0.039$ ,  $P_{\text{sm/sm+apc}}=0.014$ ). DAPI staining in blue identifies the cell nuclei. Scale bars = 10  $\mu\text{m}$ . **(f–i)** Images of dihydrorhodamine (DHR) staining and graphs showing the mean ( $\pm$  s.e.m.) DHR fluorescence that reflects the reactive oxygen species (ROS) levels in: **(f)** the hippocampus of 4-month-old wt and ASMko mice ( $n=5$ , Student's *t*-test,  $P=0.035$ ). **(g)** 12 DIV wt and ASMko neurons ( $n=80$  neurons from three cultures, Mann–Whitney *U*-test,  $P=0.0004$ ). **(h)** 12 DIV wt neurons untreated (control), treated with SM (SM), treated with apocynin (APC), or treated with SM and apocynin (SM+APC) ( $n=100$  neurons from five cultures, two-way ANOVA followed by MSD:  $P_{\text{ctl-sm}}=0.004$ ,  $P_{\text{sm-sm+apc}}=0.0006$ ); **(i)** 12 DIV wt neurons untreated (control), treated with SM (SM), or treated with SM and the neutral and acid sphingomyelinase (ASM) inhibitors GW4869 and Siramesine (GW4869+Sir+SM) ( $n=70$  neurons from three cultures, two-way ANOVA followed by MSD:  $P_{\text{ctl-sm}}=0.0008$ ,  $P_{\text{ctl-smGWsir}}=0.0005$ ). DAPI staining in blue identifies the cell nuclei. Scale bars **f–i** = 10  $\mu\text{m}$ .

neurons there was a significant 22% increase in intracellular steady state calcium concentrations compared with wt neurons. In addition, ASMko neurons took 36% longer to reach a plateau after calcium spike induction by the addition of 30 mM KCl (Figure 2a). To determine whether SM accumulation mediated these calcium alterations, we added SM to wt neurons (40  $\mu\text{M}$  for 16 h), which induced a 31% increase in steady state calcium and extended the time to reach a calcium plateau after stimuli by 32% (Figure 2b). Autofluorescence measurements and small deviations between cultures ( $<10\%$ , see graphs in Figures 2a and b) indicated that the observed increments were not due to SM-induced autofluorescence or to neuronal culture variability from genotype or condition. Together, these results indicate that a loss of calcium homeostasis is a characteristic feature of ASMko neurons and high SM levels induce this alteration.

As high calcium levels can promote oxidative stress, we analyzed whether this increase in calcium underlies oxidative stress in ASMko neurons. Incubating ASMko neurons in the calcium chelator BAPTA-AM<sup>32</sup> (10  $\mu\text{M}$ ) for 16 h reduced intracellular calcium levels by 31% and restored ROS levels in these neurons to wt levels (Figure 2c). To verify that high levels of SM trigger calcium-mediated oxidative stress, wt neurons previously incubated for 30 min with BAPTA-AM (10  $\mu\text{M}$ ) were exposed to SM (40  $\mu\text{M}$ ) for 16 h in the continued presence of the calcium chelator. The presence of BAPTA-AM prevented the SM-induced increase of ROS in wt neurons (Figure 2d). These results indicate that high SM levels disrupt calcium homeostasis, which induce oxidative stress in hippocampal neurons.

#### PMCA impairment mediates increased calcium and oxidative stress in hippocampal neurons from ASMko mice

Next, we determined how increased SM levels augment intracellular calcium in ASMko neurons. In non-neuronal cells, SM accumulation impairs the lysosomal calcium channel Mucolipin TRP1 (TRPML1) by reducing lysosomal calcium release in fibroblasts of NPA patients.<sup>33</sup> However, such a defect would only account for increased lysosomal, but not cytosolic, calcium levels. The sarco/endoplasmic reticulum calcium ATPase (SERCA) transfers calcium from the cytosol to the endoplasmic reticulum,<sup>34</sup> and its expression is decreased in the cerebellum of ASMko mice.<sup>35</sup> However, this defect seems independent of SM and cerebellar-specific. Given the accumulation of SM in the plasma membrane of ASMko hippocampal neurons,<sup>14</sup> we examined the two calcium extrusion systems at this cellular site: the  $\text{Na}^+/\text{Ca}^{2+}$  exchanger (NCX) and the PMCA.<sup>36,37</sup> We perfused isosmotic KCl over 1 min, followed by its removal by perfusion with a KCl-free buffer. After each isosmotic KCl stimulus, we detected defects in calcium buffering in ASMko neurons relative to wt neurons (Figure 3a). We performed the same experiment using  $\text{Na}^+$ -free medium to prevent NCX activity. Despite the reduced calcium peak after

each stimulus, wt neurons could compensate for the lack of  $\text{Na}^+$ -exchanger activity (Figure 3b). By contrast, impaired calcium buffering after each KCl addition was exacerbated in ASMko neurons (Figure 3b). As differences in calcium homeostasis occurred in the absence of NCX-dependent calcium extrusion between ASMko and wt neurons, this calcium extrusion system does not participate in the calcium imbalance of ASMko neurons. To assess the contribution of PMCA, we measured its activity in hippocampal extracts using an enzymatic assay based on the sequential inhibition of PMCA and SERCA with vanadate and thapsigargin, respectively.<sup>19</sup> The activity of PMCA, but not that of SERCA, was reduced by 30% in ASMko relative to wt extracts (Figures 3c and d) suggesting PMCA mediates the calcium imbalance.

#### An altered lipid environment causes PMCA deficient activity

To determine the specific mechanism underlying PMCA impairment, we measured PMCA levels in hippocampal membrane extracts and found no significant differences between ASMko and wt mice in western blots (Figure 3e). PMCA activity in brain membranes is enhanced in sphingolipid-cholesterol enriched raft domains,<sup>38</sup> though excessive SM-cholesterol levels can diminish PMCA activity in liposomes.<sup>39</sup> We hypothesized that the anomalous lipid environment mediates the deficit in PMCA activity observed in ASMko brains. So, we monitored pump activity in the presence of a low concentration of saponin, which mildly disrupts membranes by extracting lipids. The differences in PMCA activity between wt and ASMko hippocampal extracts were abolished by decreasing lipid involvement (Figure 3f, compare with Figure 3c). The increase in lipids produced by culturing wt neurons in the presence of SM (40  $\mu\text{M}$ ) for 16 h reduced PMCA activity by 25% (Figure 3g), but it did not affect SERCA (Figure 3h, see also Figure 3d) consistent with the unaltered SERCA activity in ASMko neurons.

We then assessed whether PMCA raft partitioning was altered in ASMko cells. ASMko and wt-cultured hippocampal neurons were cold extracted in 1% Triton X-100 and centrifuged to discriminate between detergent resistant membranes in the pellet, corresponding to rafts, and detergent soluble material in the supernatant, corresponding to non-rafts. Using western blots probed with an antibody against PMCA, we found a significant shift in PMCA localization from the detergent-insoluble raft fraction (59% reduction) to the soluble non-raft fraction in ASMko compared with wt extracts (Figure 3i). The constant levels of the raft marker Flotillin1 indicated this effect was specific to PMCA (Figure 3i). To further test whether PMCA was displaced from raft lipid domains, we analyzed co-localization of PMCA and the raft marker GM1 in cultures of ASMko and wt hippocampal neurons using immunofluorescence.<sup>14</sup> In ASMko neurons, co-localization of PMCA with fluoresceinated cholera toxin subunit B, which binds to GM1, was 22% weaker than in wt neurons (Figure 3j). Moreover,

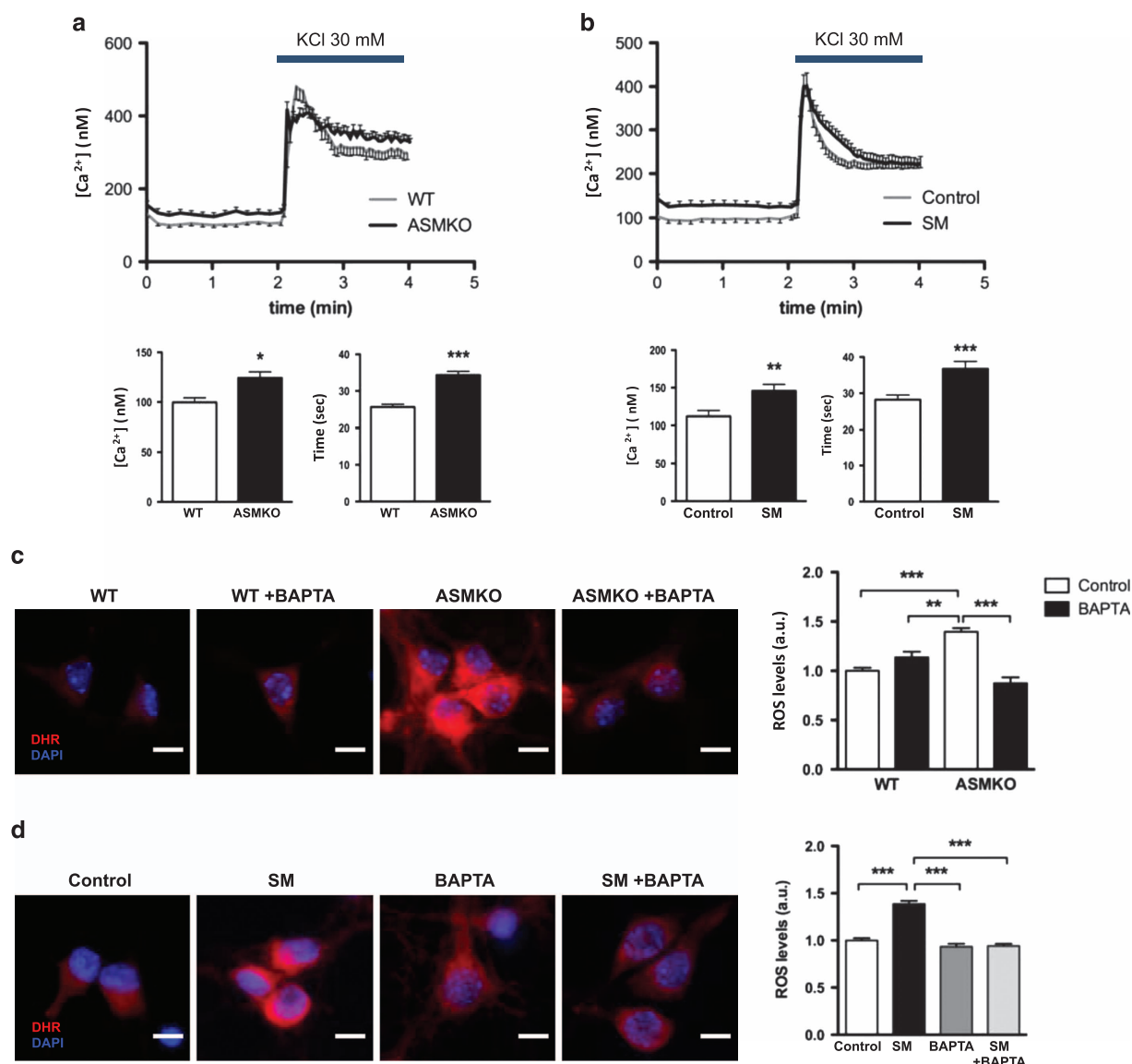


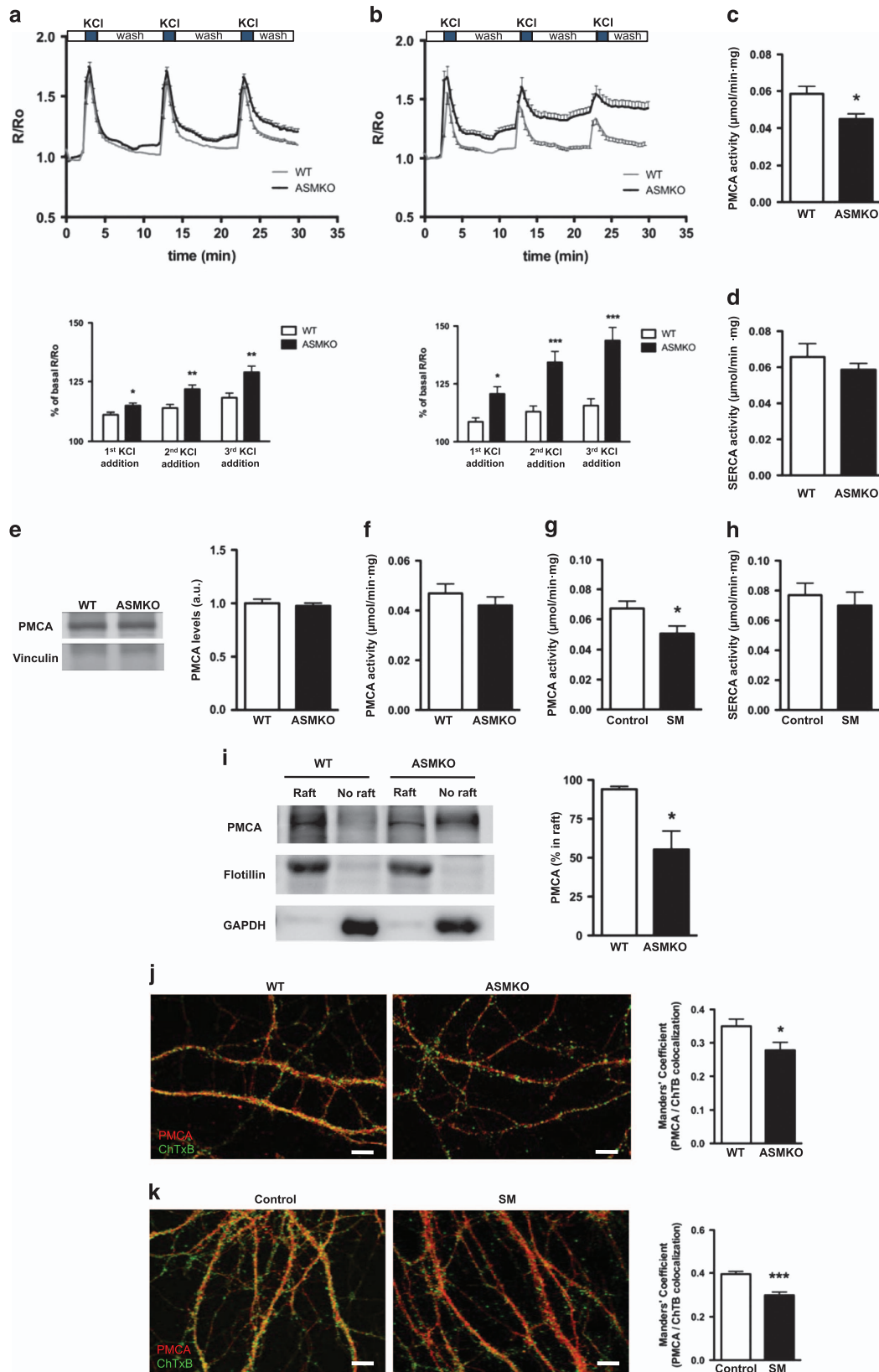
**Figure 2.** The sphingomyelin (SM)-induced increase in intracellular calcium induces oxidative stress in ASM knockout (ASMko) hippocampal neurons. **(a,b)** Diagrams showing the calcium concentration (in nM) over time (in min) in wild-type (wt) and ASMko-cultured neurons **(a)**, and in wt neurons treated or not with SM **(b)**. Graphs show the mean ( $\pm$ s.e.m.) basal calcium levels (Mann–Whitney *U*-test,  $P_{ko}=0.008$ ,  $P_{wt+sm}=0.002$ ) or time to return to the basal calcium levels after stimulation with 30 mM KCl (Mann–Whitney *U*-test,  $P_{ko}=0.0005$ ,  $P_{wt+sm}=0.0001$ ) ( $n$  = at least 50 neurons from four cultures). **(c)** Dihydrorhodamine (DHR) staining in 12 DIV wt and ASMko neurons maintained in the presence or absence of BAPTA-AM. **(d)** DHR staining in 12 DIV wt neurons maintained in the presence or absence of SM and BAPTA-AM. The graphs in **c** and **d** show the mean ( $\pm$ s.e.m.). DHR fluorescence that reflects the reactive oxygen species (ROS) levels **(c)**,  $n=80$  neurons from three cultures, Mann–Whitney *U*-test followed by Bonferroni *post hoc*,  $P_{wt/ko}=0.0004$ ,  $P_{wt-bapta/ko}=0.003$ ,  $P_{ko/ko-bapta}=0.00015$ . **(d)**  $n=100$  neurons from five cultures, two-way ANOVA followed by Games–Howell *post hoc*,  $P_{ctl/sm}=0.0003$ ,  $P_{sm/bapta}=0.0002$ ,  $P_{sm/sm+bapta}=0.00017$ ). DAPI staining in blue identifies the cell nuclei. Scale bars = 10  $\mu$ m.

a similar reduction (25%) in co-localization between PMCA and GM1 occurred in wt hippocampal neurons after adding SM (Figure 3k). Together, these data indicate that SM accumulation in ASMko neuronal membranes hinders PMCA activity, which is accompanied by its displacement from rafts.

SAHA, a histone deacetylase inhibitor, enhances PMCA levels in ASMko-cultured neurons and prevents the PMCA-dependent increase in calcium and oxidative stress

As histone deacetylase inhibitors (HDACis) upregulate PMCA to enhance calcium clearance in cancer cells,<sup>40</sup> we hypothesized that HDACis increase PMCA levels and compensate for its activity loss

in ASMko neurons. We evaluated the effects of the HDACis, suberoylanilide hydroxamic acid (SAHA or vorinostat), as this drug crosses the blood–brain barrier<sup>22</sup> and is approved for lymphoma treatment in humans.<sup>41</sup> We tested whether SAHA affected the ASMko neuron phenotype *in vitro*. SAHA application for 4 days (4 or 8  $\mu$ M) caused a dose dependent increase in PMCA protein levels (40 and 70%, respectively) in ASMko-cultured hippocampal neurons (Figure 4a). Treatment of ASMko neurons with SAHA (8  $\mu$ M) restored calcium homeostasis, reducing steady state calcium levels (24% lower) and the time required to reach a plateau after stimulus with KCl (20% lower: Figure 4b). SAHA also decreased ROS in ASMko neurons by 34% (Figure 4c). The effects of SAHA on ROS and intracellular calcium levels were PMCA



dependent, as they were abolished in the presence of Caloxin 2a1, a specific inhibitor of PMCA activity<sup>20,21</sup> (Figures 4c and d).

To further delineate the specific involvement of PMCA in the effects of SAHA, we silenced PMCA using a lentiviral vector

expressing shRNA against PMCA2, the most abundant PMCA isoform in the hippocampus. Viral infectivity reached 60% of the cultured neurons as identified by GFP expression and diminished PMCA levels by 53% as determined by western blotting of total

**Figure 3.** Deficient plasma membrane calcium ATPase (PMCA) activity induced by sphingomyelin (SM) contributes to the altered calcium homeostasis in ASM knockout (ASMko)-cultured neurons and in the hippocampus. Superfusion experiments using normal (a) or Na<sup>+</sup>-free media (b) for Fura2-AM loaded wild-type (wt) and ASMko neurons. Traces of the Fura2-AM signal as the ratio of the fluorescence emitted at 340 and 380 nm normalized to the initial Fura2-AM ratio ( $R/R_0$ ). The bars indicate the moment and duration of KCl addition and its removal by washing with KCl-free buffer. The graphs show the mean ( $\pm$  s.e.m.) Fura2-AM signal expressed relative to the initial signal in normal (a) and Na<sup>+</sup>-free media (b) ( $n =$  at least 50 neurons from three cultures, Student's  $t$ -test: normal media  $P_{\text{FirstKCl}} = 0.014$ ,  $P_{\text{SecondKCl}} = 0.001$ ,  $P_{\text{ThirdKCl}} = 0.003$ ; Na<sup>+</sup>-free media  $P_{\text{FirstKCl}} = 0.009$ ,  $P_{\text{SecondKCl}} = 0.0002$ ,  $P_{\text{ThirdKCl}} = 0.00003$ ). (c,d) The graphs show the mean ( $\pm$  s.e.m.) PMCA (c) and SERCA (d) activity in  $\mu\text{mol ATP}/\text{min}\cdot\text{mg}$  protein in hippocampal extracts from wt and ASMko mice ( $n = 8$ , Student's  $t$ -test,  $P_{\text{PMCA}} = 0.015$ ,  $P_{\text{SERCA}} = 0.189$ ). (e) Western blot of hippocampal extracts from 4-month-old wt and ASMko mice probed for PMCA and vinculin. The graph shows the mean ( $\pm$  s.e.m.) PMCA levels normalized to vinculin ( $n = 7$ , Student's  $t$ -test:  $P = 0.618$ ). (f) The graph shows the mean ( $\pm$  s.e.m.) PMCA activity in ASMko and wt mice hippocampal extracts in the presence of saponin ( $n = 5$ , Mann–Whitney  $U$ -test:  $P = 0.525$ ). (g,h) The graphs show the mean ( $\pm$  s.e.m.) PMCA (g) or SERCA (h) activity ( $\mu\text{mol ATP}/\text{min}\cdot\text{mg}$ ) in cultured wt neurons maintained in the presence or absence of SM ( $n = 8$ , Student's  $t$ -test,  $P_{\text{PMCA}} = 0.017$ ). (i) PMCA western blot of raft and non-raft fractions from ASMko and wt-cultured hippocampal neurons. Graph shows the mean ( $\pm$  s.e.m.) percentage of total PMCA in the raft fractions ( $n = 4$  independent cultures, Student's  $t$ -test,  $p = 0.018$ ). Flotillin1 and GAPDH were used as markers for raft and non-raft fractions, respectively. (j,k) Merged images of 12 DIV hippocampal neurons from wt and ASMko mice (j), and from wt mice treated with SM (k), stained with an antibody against PMCA (red) and with fluoresceinated cholera toxin subunit B (green) that binds to GM1. The graphs show the mean ( $\pm$  s.e.m.) coefficient of co-localization between PMCA and cholera toxin subunit B ( $n =$  at least 50 neurons from three cultures, Student's  $t$ -test:  $P_{\text{wt/ko}} = 0.035$ ,  $P_{\text{cont/sm}} = 0.000008$ ). Scale bars = 10  $\mu\text{m}$ .

extracts from hippocampal cultures (Figure 4e). Although SAHA reduced ROS and calcium levels in ASMko neurons infected with a scrambled shRNA used as a control, it had no significant effect on ASMko neurons infected with sh-PMCA2 (Figures 4f and g). When wt neurons were exposed to SAHA (8  $\mu\text{M}$ ) for 2 days before adding SM, there was a clear reduction in lipid-induced ROS formation (Figure 4h). Taken together, these data indicate that SAHA dampens SM-induced calcium increase and oxidative stress in a PMCA-dependent manner in hippocampal neurons.

Oral SAHA administration increases PMCA levels and prevents oxidative stress, behavioral deficits and neuronal death in ASMko mice

Given the efficacy of SAHA in enhancing PMCA activity and in preventing calcium imbalance and oxidative stress in ASMko-cultured neurons, we tested the effects of this compound *in vivo*. We administered SAHA complexed to 2-hydroxypropyl- $\beta$ -cyclodextrin (HOP- $\beta$ -CDX), an agent that enhances the poor aqueous solubility of SAHA and its blood–brain barrier penetration, to 2-month-old ASMko and wt mice.<sup>22</sup> Mice received a dose of 100 mg of SAHA per kg of body weight per day in the drinking water over 1.5 months, and their water consumption was monitored to confirm that all mice received similar amounts of the drug (Supplementary Figure S4). SAHA administration had no effect on SM levels in hippocampal extracts (Supplementary Figure S5a), but it did efficiently inhibit histone deacetylation in western blots probed for histone 3 and one of its acetylated sites (Supplementary Figure S5b). SAHA treatment also significantly increased PMCA protein levels by 20% in hippocampal membranes of ASMko and wt mice (Figures 5a and b).

We analyzed the effects of SAHA administration on oxidative stress by measuring ROS levels in hippocampal slices by DHR staining. Although we found no significant changes in the amount of ROS in wt mice, a 60% reduction in ROS was detected in ASMko-treated mice (Figure 5c). The effects of SAHA on PMCA and ROS levels were not observed in mice that received only HOP- $\beta$ -CDX, indicating they were specifically induced by SAHA (Supplementary Figures S6a and b).

To determine the functional effects of SAHA, we analyzed hippocampal dependent working memory, which is impaired in ASMko mice (Figure 5d). ASMko mice spent less time exploring the novel arm in the Y-maze test (25%) than wt mice (46%), but performance returned to wt levels following the administration of SAHA (45%), indicative of improved working memory (Figure 5d). SAHA had no effect on working memory performance of wt mice (Figure 5d).

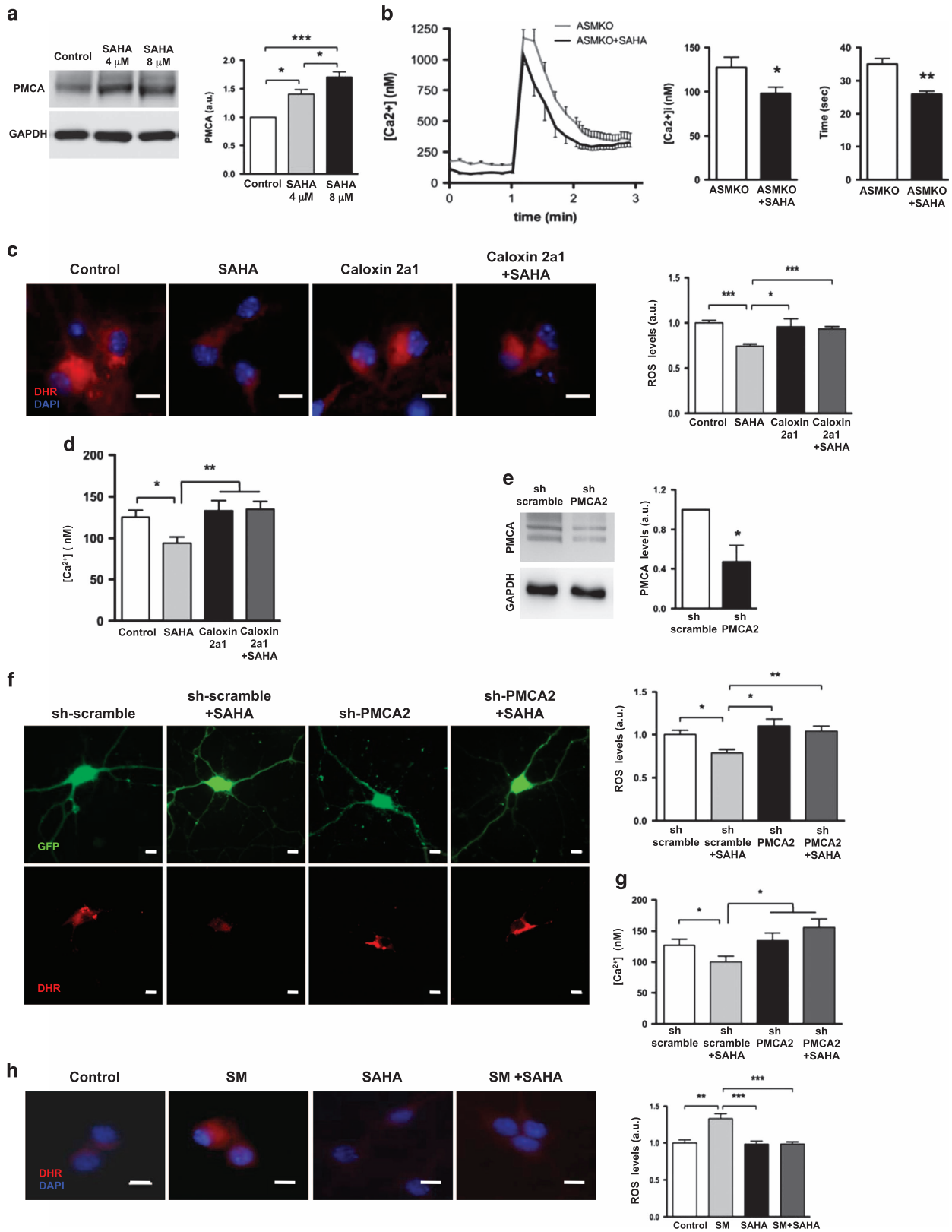
Calcium-induced oxidative stress<sup>31</sup> causes neurotoxicity, so we determined whether SAHA prevented neuronal death in ASMko

mice. At 4 months of age, there is no neurodegeneration in the hippocampus of ASMko mice as determined by fractin immunostaining (Supplementary Figure S7). Therefore, SAHA treatment had no effect on neurodegeneration as confirmed by unchanged levels of cleaved caspase-3 fragments (Supplementary Figure S7). However, Purkinje cells of the cerebellum had almost completely disappeared at that age in these mice<sup>42</sup> (Supplementary Figure S8). So, we monitored the effects of SAHA treatment on cerebellar neuron survival. Oral SAHA administration enhanced PMCA levels in cerebellar membranes of ASMko mice (Figure 5e). Immunohistological analysis using the Purkinje cell marker calbindin indicated that neuronal survival did not improve significantly in the anterior lobes, as extensive neuronal loss was already evident in this area at 2 months of age when the treatment began.<sup>43</sup> However, survival was significantly enhanced (67%) in the mid and posterior lobes in SAHA-treated ASMko mice (Figure 5f; Supplementary Figure S8). To determine whether this treatment had functional consequences, we assayed motor coordination in a Rotarod test. In ASMko mice that received SAHA, the latency to fall from the rod increased 50 and 35% in the third and fourth trials, respectively, than in untreated mice, indicating improved motor coordination (Figure 5g). SAHA administration did not significantly affect Purkinje cell number or motor coordination in wt mice (Figures 5f and g; Supplementary Figure S8). Together, these results show the efficacy of oral SAHA administration to increase brain PMCA levels and to prevent oxidative stress, neurodegeneration and behavioral deficits in ASMko mice.

## DISCUSSION

Here, we identify neuronal oxidative stress as a pathological hallmark of NPA. Using the ASMko mouse model for NPA, we find accumulation of SM, altered PMCA activity and disrupted calcium homeostasis. We demonstrate that excessive SM accumulation at the neuronal plasma membrane causes unusually high intracellular calcium levels in these cells, which increases oxidative stress and neuronal death. Perturbations in the activity of the plasma membrane calcium pump PMCA underlie the increased calcium levels. These results demonstrate that altered calcium imbalance is a determinant modification that lies upstream of oxidative stress in ASM-deficient neurons. We identify a non-invasive pharmacological strategy that may prevent the brain anomalies accompanying ASM deficiency, as this therapeutic strategy can successfully ameliorate features of this disease both *in vitro* and *in vivo*.

SM is enriched in neuronal membranes, where it has various functions. Indeed, correct SM levels are necessary to secure axonal polarity and synaptic plasticity.<sup>12,14,15,44</sup> We demonstrate the relevance of SM in neuronal calcium homeostasis through



regulating calcium efflux at the plasma membrane. Our results show that the antiporter plasma membrane protein NCX does not mediate SM-induced calcium anomalies; rather high SM levels significantly diminish the activity of PMCA. As a plasma membrane calcium pump, PMCA is better candidate to maintain low resting

cellular calcium concentrations due to its high affinity for calcium,<sup>37</sup> in contrast to the low calcium affinity of NCX. The effect of SM on PMCA may occur through a direct effect of this lipid on PMCA folding<sup>39</sup> or indirectly by changing its interactions with binding proteins<sup>45</sup> such as altering raft

**Figure 4.** Incubating ASMko-cultured hippocampal neurons in SAHA increases plasma membrane calcium ATPase (PMCA) levels, whereas reducing calcium and reactive oxygen species (ROS) levels and decreasing sphingomyelin (SM)-induced oxidative stress. **(a)** Western blots of extracts from ASM knockout (ASMko)-cultured neurons maintained in the presence or absence of the indicated concentrations of SAHA and probed for PMCA and GAPDH. The graph shows the mean ( $\pm$  s.e.m.) PMCA levels normalized to GAPDH ( $n=3$  cultures, one-way ANOVA followed by minimum significant difference (MSD):  $P_{\text{ctl/saha4}}=0.006$ ,  $P_{\text{ctl/saha8}}=0.0005$ ,  $P_{\text{saha4/saha8}}=0.025$ ). **(b)** The diagram shows the calcium concentration (in nM) over time (in min) in ASMko-cultured neurons maintained in the presence or absence of SAHA (8  $\mu\text{M}$ ). The graphs show the mean ( $\pm$  s.e.m.) basal calcium (Student's  $t$ -test,  $P=0.03$ ) and the time to return to the basal calcium levels after stimulation with 30 mM KCl (Mann–Whitney  $U$ -test:  $P=0.004$ ;  $n$  = at least 50 neurons from three cultures). **(c)** Dihydrorhodamine (DHR) staining in 12 DIV ASMko neurons maintained in the presence or absence of SAHA (8  $\mu\text{M}$ ) and in the presence or absence of Caloxin 2a1. The graph shows the mean ( $\pm$  s.e.m.) fluorescence associated to DHR indicative of ROS ( $n=75$  neurons from three cultures, two-way ANOVA followed by Games–Howell *post hoc*:  $P_{\text{Control/saha}}=0.00003$ ,  $P_{\text{ko/kosaha}}=0.0003$ ,  $P_{\text{saha/caloxin}}=0.042$ ,  $P_{\text{saha/saha+caloxin}}=0.00007$ ). **(d)** Basal calcium levels in neurons treated or not with SAHA in the presence or absence of Caloxin 2a1 (mean ( $\pm$  s.e.m.);  $n$  = at least 50 neurons from three cultures, two-way ANOVA followed by Games–Howell *post hoc*,  $P_{\text{Control/saha}}=0.010$ ,  $P_{\text{saha/caloxin}}=0.004$ ,  $P_{\text{saha/saha+caloxin}}=0.001$ ). **(e)** Western blot of total extracts from hippocampal neuron cultures infected with lentiviral vectors expressing shRNAs against PMCA2 or a scrambled shRNA and probed for PMCA and GAPDH. The graph shows mean PMCA levels ( $\pm$  s.e.m.) normalized to GAPDH;  $n=3$ , Student's  $t$ -test,  $P=0.038$ ). **(f)** DHR staining (lower panels) in ASMko neurons infected with lentiviral vectors expressing shRNAs against PMCA2 or a scrambled shRNA and maintained in the presence or absence of SAHA (8  $\mu\text{M}$ ). Infected neurons in the cultures were identified by GFP expression (upper panels). The graph shows the mean ( $\pm$  s.e.m.) fluorescence associated to DHR, indicative of ROS ( $n=60$  neurons from three cultures, two-way ANOVA followed by MSD:  $P_{\text{scrambled/saha}}=0.011$ ,  $P_{\text{scrambled+saha/shPMCA2}}=0.005$ ,  $P_{\text{scrambled+saha/shPMCA2+saha}}=0.004$ ) **(g)** Basal calcium levels in neurons infected with lentiviral vectors expressing shRNAs against PMCA2 or scramble shRNA and treated or not with 8  $\mu\text{M}$  SAHA (mean ( $\pm$  s.e.m.);  $n$  = at least 20 neurons from three cultures, two-way ANOVA followed by Games–Howell *post hoc*,  $P_{\text{scramble/scramble+saha}}=0.042$ ,  $P_{\text{scramble+saha/shPMCA2}}=0.047$ ,  $P_{\text{scramble+saha/shPMCA2+saha}}=0.001$ ). **(h)** DHR staining in 12 DIV wt neurons treated or not with SM and in the presence or absence of SAHA (8  $\mu\text{M}$ ). Image shows fluorescence associated to DHR staining indicating ROS (mean ( $\pm$  s.e.m.);  $n=50$  neurons from three cultures, two-way ANOVA followed by Games–Howell:  $P_{\text{ctl/sm}}=0.001$ ,  $P_{\text{sm/saha}}=0.0003$ ,  $P_{\text{sm/sm+saha}}=0.0003$ ). DAPI staining in blue identifies cell nuclei. Scale bars = 10  $\mu\text{m}$ .

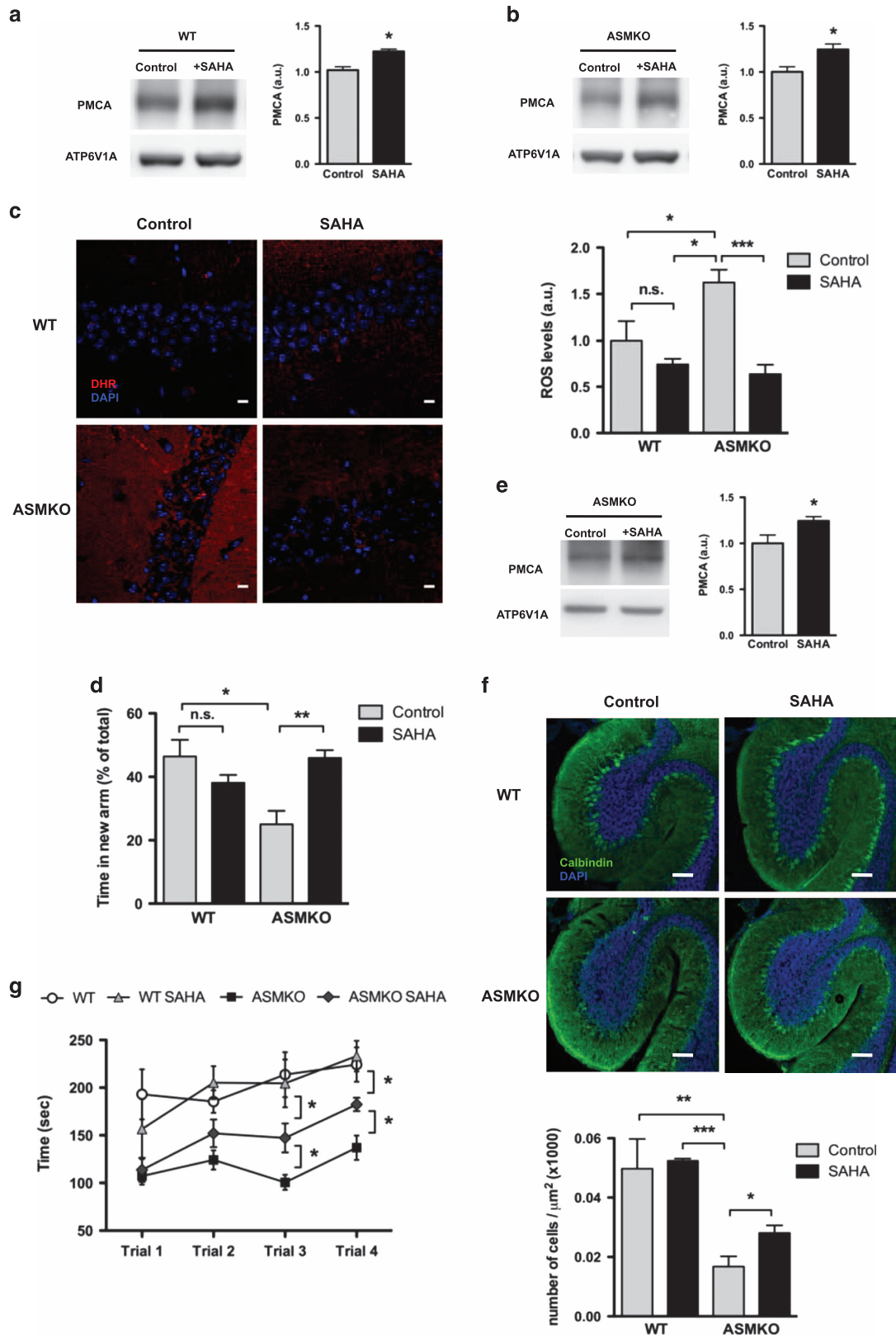
compartmentalization. SM may also alter actin polymerization, as reported in ASMko neurons,<sup>14</sup> which could alter PMCA activity.<sup>45</sup> Moreover, oxidative stress triggered by PMCA deficiency could engage a negative feedback loop that exaggerates the effects of this calcium pump due to its high sensitivity to ROS-induced cross-linking.<sup>46</sup>

Alterations in intracellular calcium concentrations likely impair important physiological events in ASM-deficient neurons regardless of the specific mechanisms mediating PMCA deficiency. These mechanisms could affect signal transduction pathways<sup>47,48</sup> and membrane repair processes. In fact, defective plasma membrane repair does occur in ASM-deficient cells.<sup>9</sup> ASM translocation to the plasma membrane by calcium-dependent lysosomal exocytosis converts SM to ceramide to trigger endocytosis and wound closure.<sup>49,50</sup> Our data suggests that the calcium imbalance associated with ASM deficiency impairs conversion of SM to ceramide at the plasma membrane and dysregulate calcium-dependent lysosomal exocytosis in ASM-deficient cells to hinder cellular repair responses. Decreased ability to adequately repair transmembrane pores formed by microbial toxins could explain why NPA patients are especially vulnerable to infection.<sup>50,51</sup>

Although LSDs may have different genetic origins, they share features, such as disrupted calcium homeostasis, that support the use of common therapeutic strategies. However, the molecular mechanisms underlying the calcium imbalance in each LSD may differ and involve distinct lipids. An increase in cytosolic calcium characterizes Gaucher and Sandhoff diseases, whereby the accumulation of glucosylceramide or ganglioside affects ER calcium channels.<sup>52–54</sup> High levels of the ganglioside GM1 alter mitochondrial calcium homeostasis in GM1 gangliosidosis,<sup>55</sup> whereas sphingosine storage reduces lysosomal calcium levels in NPC.<sup>56</sup> Intriguingly, SM impairs TRPML1-mediated lysosomal calcium release<sup>33</sup> in fibroblasts from NPC and NPA patients, which suggests that enhanced lysosomal calcium release could be beneficial in these conditions. Indeed, this approach has had some positive effects in NPC fibroblasts where cytosolic calcium levels are reduced.<sup>35</sup> However, the increase in intracellular calcium we observe in ASMko neurons, provoked by defects in the plasma membrane calcium extrusion systems, raises concern about applying the same strategy to NPA. Impaired calcium uptake via SERCA is specifically found in microsomes isolated from the

cerebellum of ASMko mice.<sup>35</sup> Although the reported defects in ER calcium channels enriched in this brain area were mediated by Purkinje cell loss and not due to sphingolipid storage.<sup>35</sup> Here, we demonstrate excess SM impairs PMCA activity to mediate the calcium imbalance in ASMko hippocampal neurons. This finding indicates that the lack of a lysosomal enzyme in LSDs facilitates alterations in calcium regulation at the plasma membrane. Enhancing PMCA activity reduces the deleterious consequences of calcium imbalances not only in the hippocampus but also in the cerebellum. Indeed, preventing Purkinje cell death by administering SAHA reveals that perturbed calcium homeostasis is a key determinant of neurodegeneration in the NPA mouse model.

A more detailed understanding of the molecular mechanisms that disrupt calcium homeostasis and their functional consequences in each LSD will establish a framework to develop common and disease-specific therapeutic strategies. Treatment with deacetylase inhibitors has proven successful in cellular models for NPC,<sup>57,58</sup> although this treatment targeted extending the half-life of the cholesterol transport protein Npc1, which is mutated in NPC and did not specifically modify the calcium imbalance. Although SAHA treatment in ASMko mice may have additional effects aside from activation of PMCA, our results demonstrate its efficacy in increasing PMCA levels and preventing oxidative stress in a PMCA-dependent manner. Chronic treatment with SAHA can enhance memory formation in wt mice in contextual fear conditioning assays.<sup>59</sup> However, we used a different behavioral assay that did not reveal effects of SAHA treatment on the cognitive abilities of wt mice. One explanation for this discrepancy is the extent of inhibition of HDACs achieved in our experimental paradigm. Pharmacokinetic studies indicate that HDAC2, which is critically involved in fear memory, shows the highest  $\text{IC}_{50}$  for SAHA compared with other HDACs.<sup>60</sup> Nevertheless, the fact that SAHA does improve memory in ASMko mice with altered neuronal calcium homeostasis, but not wt mice, suggests that the SAHA-induced cognitive benefits are not due to enhanced synaptic activity but rather to the rescue of the endogenous calcium imbalance. On the other hand, the fact that SAHA does not affect the ROS levels in wt mice could reflect the low oxidative stress in the brains of these mice at 4 months of age, which would render any further reduction in ROS difficult to detect.



Finally, this study demonstrates how specific pathological features of NPA can be prevented without directly addressing the primary causes of this disease—ASM deficiency and SM accumulation (Supplementary Figure S5). Further, our study supports the suitability of symptomatic therapies for NPA, for

which no treatments currently exist. Our data show that SAHA is an effective therapy even after disease onset. In fact, we began treatment in ASMko mice at 2 months of age after we detected high levels of SM in the brain and motor impairment. This result is critical for NPA, when newborns appear normal but

**Figure 5.** Oral SAHA administration increases brain plasma membrane calcium ATPase (PMCA) levels, reduces oxidative stress, improves behavioral deficits and prevents neurodegeneration in ASM knockout (ASMko) mice. **(a,b)** Western blot of hippocampal membrane extracts from wt **(a)** and ASMko **(b)** mice orally administered SAHA complexed to HOP- $\beta$ -CDX (SAHA) or HOP- $\beta$ -CDX (control), and probed for PMCA and ATP6V1A. The graphs showing the mean ( $\pm$  s.e.m.) PMCA levels normalized to ATP6V1A ( $n = 7$ , Student's *t*-test:  $P_{wt} = 0.014$ ,  $P_{ko} = 0.011$ ). **(c)** Dihydrorhodamine (DHR) staining of the hippocampus from control and SAHA-treated wild-type (wt) and ASMko mice. The graph on the right shows the mean ( $\pm$  s.e.m.) DHR fluorescence, indicative of ROS ( $n = 7$ , two-way ANOVA followed by minimum significant difference (MSD):  $P_{wt/ko} = 0.015$ ,  $P_{wt-saha/ko} = 0.007$ ,  $P_{ko/ko-saha} = 0.0004$ ; n.s. not significant). DAPI staining in blue identifies cell nuclei. Scale bars = 10  $\mu$ m. **(d)** Y-maze test on control and SAHA-treated wt and ASMko mice. The graph shows the relative time spent in the novel arm (mean ( $\pm$  s.e.m.));  $n = 7$ , two-way ANOVA followed by MSD:  $P_{wt/ko} = 0.024$ ,  $P_{wt/wt-saha} = 0.5$ ,  $P_{ko/ko-saha} = 0.003$ ). **(e)** Western blot of cerebellar membrane extracts from control and SAHA-treated ASMko mice probed for PMCA and ATP6V1A. The graphs show the mean ( $\pm$  s.e.m.) PMCA levels normalized to ATP6V1A ( $n = 7$ , Student's *t*-test:  $P = 0.032$ ). **(f)** Calbindin immunostaining of Purkinje cells in posterior lobe X of the cerebellum from control and SAHA-treated wt and ASMko mice. Calbindin positive cells in the mid and posterior lobes of the cerebellum (VI–X) per area unit (mean ( $\pm$  s.e.m.));  $n = 7$ , two-way ANOVA followed by MSD:  $P_{wt/ko} = 0.001$ ,  $P_{wt-saha/ko} = 0.0005$ ,  $P_{ko/ko-saha} = 0.049$ ). DAPI staining in blue identifies the cell nuclei. Scale bars = 100  $\mu$ m. **(g)** Rotarod test in control and SAHA-treated wt and ASMko mice. The graph shows mean ( $\pm$  s.e.m.) time (in seconds) spent before falling from the rod in four consecutive accelerating trials;  $n = 7$ , two-way ANOVA followed by MSD:  $P_{wt/ko-saha3} = 0.034$ ,  $P_{ko/ko-saha3} = 0.037$ ,  $P_{wt/ko-saha4} = 0.028$ ,  $P_{ko/ko-saha4} = 0.038$ .

clinical symptoms do not appear until 3–6 months of age. We believe our results will expand the therapeutic time window for this rapidly progressive disease, with little to no clinical treatment options.

### CONFLICT OF INTEREST

The authors declare no conflict of interest.

### ACKNOWLEDGMENTS

We thank the Wylder Nation Foundation for kindly donating the NPA brain tissue, EH Schuchman (Mount Sinai School of Medicine, New York) for providing us with the ASMko mice, AM Mata (Universidad de Extremadura) and JJ Lucas (CBMSO) for technical advice, and C. Aragón, B. López-Corcuera and E. Núñez for providing the Caloxin 2a1 and for their advice on its use. This work was financed by grants from the Ministerio Español de Ciencia e Innovación (SAF2014-57539-R and CSD2010-00045) and the Fundación Niemann Pick España to MDL, and by an institutional grant to the CBMSO from the Fundación Ramón Areces. APC holds a predoctoral fellowship (FPU) funded by the Ministerio Español de Ciencia e Innovación. We thank Life Science Editors for editing services.

### REFERENCES

- Vanier MT. Niemann–Pick diseases. *Handb Clin Neurol* 2013; **113**: 1717–1721.
- Schuchman EH, Desnick RJ. Niemann–Pick disease types A and B: acid sphingomyelinase deficiencies. In: Scriver CR *et al* (eds). *The Metabolic and Molecular Bases of Inherited Disease*, vol. II. McGraw-Hill: New York, NY, USA, 2001, p. 3589.
- Brady RO, Kanfer JN, Mock MB, Fredrickson DS. The metabolism of sphingomyelin. II. Evidence of an enzymatic deficiency in Niemann–Pick disease. *Proc Natl Acad Sci USA* 1996; **55**: 366–369.
- Patterson MC, Vecchio D, Prady H, Abel L, Wraith JE. Miglustat for treatment of Niemann–Pick C disease: a randomised controlled study. *Lancet Neurol* 2007; **6**: 765–772.
- Wasserstein MP, Jones SA, Soran H, Diaz GA, Lippa N, Thurberg BL *et al*. Successful within-patient dose escalation of olipudase alfa in acid sphingomyelinase deficiency. *Mol Genet Metab* 2015; **116**: 88–97.
- Stoffel W. Functional analysis of acid and neutral sphingomyelinases *in vitro* and *in vivo*. *Chem Phys Lipids* 1999; **102**: 107–121.
- Futerman AH, van Meer G. The cell biology of lysosomal storage disorders. *Nat Rev Mol Cell Biol* 2004; **5**: 554–565.
- Gabandé-Rodríguez E, Boya P, Labrador V, Dotti CG, Ledesma MD. High sphingomyelin levels induce lysosomal damage and autophagy dysfunction in Niemann Pick disease type A. *Cell Death Differ* 2014; **21**: 864–875.
- Tam C, Idone V, Devlin C, Fernandes MC, Flannery A, He X *et al*. Exocytosis of acid sphingomyelinase by wounded cells promotes endocytosis and plasma membrane repair. *J Cell Biol* 2010; **189**: 1027–1038.
- Horinouchi K, Erlich S, Perl DP, Ferlinz K, Bisgaier CL, Sandhoff K *et al*. Acid sphingomyelinase deficient mice: a model of types A and B Niemann–Pick disease. *Nat Genet* 1995; **10**: 288–293.
- Gulbins E, Palmada M, Reichel M, Lüth A, Böhmer C, Amato D *et al*. Acid-sphingomyelinase-ceramide system mediates effects of antidepressant drugs. *Nat Med* 2013; **19**: 934–941.

- Arroyo AI, Camoletto PG, Morando L, Sassoe-Pognetto M, Giustetto M, Van Veldhoven PP *et al*. Pharmacological reversion of sphingomyelin-induced dendritic spine anomalies in a Niemann Pick disease type A mouse model. *EMBO Mol Med* 2014; **6**: 398–413.
- Trovò L, Stroobants S, D'Hooge R, Ledesma MD, Dotti CG. Improvement of biochemical and behavioral defects in the Niemann–Pick type A mouse by intraventricular infusion of MARCKS. *Neurobiol Dis* 2015; **73**: 319–326.
- Galvan C, Camoletto PG, Cristofani F, Van Veldhoven PP, Ledesma MD. Anomalous surface distribution of glycosyl phosphatidyl inositol-anchored proteins in neurons lacking acid sphingomyelinase. *Mol Biol Cell* 2008; **19**: 509–522.
- Camoletto PG, Vara H, Morando L, Connell E, Marletto FP *et al*. Synaptic vesicle docking: sphingosine regulates syntaxin1 interaction with Munc18. *PLoS One* 2009; **4**: e5310.
- Vitner EB, Platt FM, Futerman AH. Common and uncommon pathogenic cascades in lysosomal storage diseases. *J Biol Chem* 2010; **285**: 20423–20427.
- Wei H, Kim SJ, Zhang Z, Tsai PC, Wisniewski KE, Mukherjee AB. ER and oxidative stresses are common mediators of apoptosis in both neurodegenerative and non-neurodegenerative lysosomal storage disorders and are alleviated by chemical chaperones. *Hum Mol Genet* 2008; **17**: 469–477.
- Gryniewicz G, Poenie M, Tsien RY. A new generation of Ca<sup>2+</sup> indicators with greatly improved fluorescence properties. *J Biol Chem* 1985; **260**: 3440–3450.
- Sepúlveda MR, Hidalgo-Sánchez M, Mata AM. A developmental profile of the levels of calcium pumps in chick cerebellum. *J Neurochem* 2005; **95**: 673–683.
- Chaudhary J, Walia M, Matharu J, Escher E, Grover AK. Caloxin: a novel plasma membrane Ca<sup>2+</sup> pump inhibitor. *Am J Physiol Cell Physiol* 2001; **280**: 1027–1030.
- de Juan-Sanz J, Núñez E, Zafra F, Berrocal M, Corbacho I, Ibáñez I *et al*. Presynaptic control of glycine transporter 2 (GlyT2) by physical and functional association with plasma membrane Ca<sup>2+</sup>-ATPase (PMCA) and Na<sup>+</sup>-Ca<sup>2+</sup> exchanger (NCX). *J Biol Chem* 2014; **289**: 34308–34324.
- Hockley E, Richon VM, Woodman B, Smith DL, Zhou X, Rosa E *et al*. Suberoylanilide hydroxamic acid, a histone deacetylase inhibitor, ameliorates motor deficits in a mouse model of Huntington's disease. *Proc Natl Acad Sci USA* 2003; **100**: 2041–2046.
- Cognato GP, Agostinho PM, Hockemeyer J, Müller CE, Souza DO, Cunha RA. Caffeine and an adenosine A(2 A) receptor antagonist prevent memory impairment and synaptotoxicity in adult rats triggered by a convulsive episode in early life. *J Neurochem* 2010; **112**: 453–462.
- Sohal RS, Brunk UT. Lipofuscin as an indicator of oxidative stress and aging. *Adv Exp Med Biol* 1989; **266**: 17–26.
- Cardozo-Pelaez F, Brooks PJ, Stedford T, Song S, Sanchez-Ramos J. DNA damage, repair, and antioxidant systems in brain regions: a correlative study. *Free Radic Biol Med* 2000; **28**: 779–785.
- Rodríguez-Lafrasse C, Vanier MT. Sphingosylphosphorylcholine in Niemann–Pick disease brain: accumulation in type A but not in type B. *Neurochem Res* 1999; **24**: 199–205.
- Luberto C, Hassler DF, Signorelli P, Okamoto Y, Sawai H, Boros E *et al*. Inhibition of tumor necrosis factor-induced cell death in MCF7 by a novel inhibitor of neutral sphingomyelinase. *J Biol Chem* 2002; **277**: 41128–41139.
- Petersen NH, Olsen OD, Groth-Pedersen L, Ellegaard AM, Bilgin M, Redmer S *et al*. Transformation-associated changes in sphingolipid metabolism sensitize cells to lysosomal cell death induced by inhibitors of acid sphingomyelinase. *Cancer Cell* 2013; **24**: 379–393.
- Franco-Villanueva A, Fernández-López E, Gabandé-Rodríguez E, Bañón-Rodríguez I, Esteban JA, Antón IM *et al*. WIP modulates dendritic spine actin cytoskeleton by

- transcriptional control of lipid metabolic enzymes. *Hum Mol Genet* 2014; **23**: 4383–4395.
- 30 Wang X, Michaelis EK. Selective neuronal vulnerability to oxidative stress in the brain. *Front Aging Neurosci* 2010; **2**: 12.
- 31 Gleichmann M, Mattson MP. Neuronal calcium homeostasis and dysregulation. *Antioxid Redox Signal* 2011; **14**: 1261–1273.
- 32 Tymianski M, Charlton MP, Carlen PL, Tator CH. Properties of neuroprotective cell-permeant Ca<sup>2+</sup> chelators: effects on [Ca<sup>2+</sup>]<sub>i</sub> and glutamate neurotoxicity *in vitro*. *J Neurophysiol* 1994; **72**: 1973–1992.
- 33 Shen D, Wang X, Li X, Zhang X, Yao Z, Dibble S *et al*. Lipid storage disorders block lysosomal trafficking by inhibiting a TRP channel and lysosomal calcium release. *Nat Commun* 2012; **3**: 731.
- 34 Pozzan T, Rizzuto R, Volpe P, Meldolesi J. Molecular and cellular physiology of intracellular calcium stores. *Physiol Rev* 1994; **74**: 595–636.
- 35 Ginzburg L, Futerman AH. Defective calcium homeostasis in the cerebellum in a mouse model of Niemann–Pick A disease. *J Neurochem* 2005; **95**: 1619–1628.
- 36 Guerini D. The Ca<sup>2+</sup> pumps and the Na<sup>+</sup>/Ca<sup>2+</sup> exchangers. *Biomaterials* 1998; **11**: 319–330.
- 37 Strehler EE, Caride AJ, Filoteo AG, Xiong Y, Penniston JT, Enyedi A. Plasma membrane Ca<sup>2+</sup>-ATPases as dynamic regulators of cellular calcium handling. *Ann N Y Acad Sci* 2007; **1099**: 226–236.
- 38 Jiang L, Bechtel MD, Galeva NA, Williams TD, Michaelis EK, Michaelis ML. Decreases in plasma membrane Ca<sup>2+</sup>-ATPase in brain synaptic membrane rafts from aged rats. *J Neurochem* 2012; **123**: 689–699.
- 39 Pang Y, Zhu H, Wu P, Chen J. The characterization of plasma membrane Ca<sup>2+</sup>-ATPase in rich sphingomyelin-cholesterol domains. *FEBS Lett* 2005; **579**: 2397–2403.
- 40 Varga K, Pászty K, Padányi R, Hegedűs L, Brouland JP, Papp B *et al*. Histone deacetylase inhibitor- and PMA-induced upregulation of PMCA4b enhances Ca<sup>2+</sup> clearance from MCF-7 breast cancer cells. *Cell Calcium* 2014; **55**: 78–92.
- 41 Bhatt S, Ashlock BM, Toomey NL, Diaz LA, Mesri EA, Lossos IS *et al*. Efficacious proteasome/HDAC inhibitor combination therapy for primary effusion lymphoma. *J Clin Invest* 2013; **123**: 2616–2628.
- 42 Sarna J, Miranda SR, Schuchman EH, Hawkes R. Patterned cerebellar Purkinje cell death in a transgenic mouse model of Niemann–Pick type A/B disease. *Eur J Neurosci* 2001; **13**: 1873–1880.
- 43 Macauley SL, Sidman RL, Schuchman EH, Taksir T, Stewart GR. Neuropathology of the acid sphingomyelinase knockout mouse model of Niemann–Pick A disease including structure–function studies associated with cerebellar Purkinje cell degeneration. *Exp Neurol* 2008; **214**: 181–192.
- 44 Ledesma MD, Brügger B, Bünning C, Wieland FT, Dotti CG. Maturation of the axonal plasma membrane requires upregulation of sphingomyelin synthesis and formation of protein–lipid complexes. *EMBO J* 1999; **18**: 1761–1771.
- 45 Vanagas L, de La Fuente MC, Dalghi M, Ferreira-Gomes M, Rossi RC, Strehler EE *et al*. Differential effects of G- and F-actin on the plasma membrane calcium pump activity. *Cell Biochem Biophys* 2013; **66**: 187–198.
- 46 Zaidi A, Michaelis ML. Effects of reactive oxygen species on brain synaptic plasma membrane Ca<sup>2+</sup>-ATPase. *Free Radic Biol Med* 1999; **27**: 810–821.
- 47 Berridge MJ, Bootman MD, Roderick HL. Calcium signalling: dynamics, homeostasis and remodelling. *Nat Rev Mol Cell Biol* 2003; **4**: 517–529.
- 48 Brini M. Plasma membrane Ca<sup>2+</sup>-ATPase: from a housekeeping function to a versatile signaling role. *Pflugers Arch* 2009; **457**: 657–664.
- 49 Corrotte M, Castro-Gomes T, Koushik AB, Andrews NW. Approaches for plasma membrane wounding and assessment of lysosome-mediated repair responses. *Methods Cell Biol* 2015; **126**: 139–158.
- 50 Idone V, Tam C, Goss JW, Toomre D, Pypaert M, Andrews NW. Repair of injured plasma membrane by rapid Ca<sup>2+</sup>-dependent endocytosis. *J Cell Biol* 2008; **180**: 905–914.
- 51 McGovern MM, Aron A, Brodie SE, Desnick RJ, Wasserstein MP. Natural history of Type A Niemann–Pick disease: possible endpoints for therapeutic trials. *Neurology* 2006; **66**: 228–232.
- 52 Korkotian E, Schwarz A, Pelled D, Schwarzmann G, Segal M, Futerman AH. Elevation of intracellular glucosylceramide levels results in an increase in endoplasmic reticulum density and in functional calcium stores in cultured neurons. *J Biol Chem* 1999; **274**: 21673–21678.
- 53 Lloyd-Evans E, Pelled D, Riebeling C, Bodenec J, de-Morgan A, Waller H *et al*. Glucosylceramide and glucosylsphingosine modulate calcium mobilization from brain microsomes via different mechanisms. *J Biol Chem* 2003; **278**: 23594–23599.
- 54 Pelled D, Lloyd-Evans E, Riebeling C, Jeyakumar M, Platt FM, Futerman AH. Inhibition of calcium uptake via the sarco/endoplasmic reticulum Ca<sup>2+</sup>-ATPase in a mouse model of Sandhoff disease and prevention by treatment with N-butyl-deoxyjirimycin. *J Biol Chem* 2003; **278**: 29496–29501.
- 55 Sano R, Annunziata I, Patterson A, Moshiaich S, Gomero E, Opferman J *et al*. GM1-ganglioside accumulation at the mitochondria-associated ER membranes links ER stress to Ca<sup>2+</sup>-dependent mitochondrial apoptosis. *Mol Cell* 2009; **36**: 500–511.
- 56 Lloyd-Evans E, Morgan AJ, He X, Smith DA, Elliot-Smith E, Silence DJ *et al*. Niemann–Pick disease type C1 is a sphingosine storage disease that causes deregulation of lysosomal calcium. *Nat Med* 2008; **14**: 1247–1255.
- 57 Pipalia NH, Cosner CC, Huang A, Chatterjee A, Bourbon P, Farley N *et al*. Histone deacetylase inhibitor treatment dramatically reduces cholesterol accumulation in Niemann–Pick type C1 mutant human fibroblasts. *Proc Natl Acad Sci USA* 2011; **108**: 5620–5625.
- 58 Munkacsy AB, Chen FW, Brinkman MA, Higaki K, Gutiérrez GD, Chaudhari J *et al*. An "exacerbate-reverse" strategy in yeast identifies histone deacetylase inhibition as a correction for cholesterol and sphingolipid transport defects in human Niemann–Pick type C disease. *J Biol Chem* 2011; **286**: 23842–23851.
- 59 Guan JS, Haggarty SJ, Giacometti E, Dannenberg JH, Joseph N, Gao J *et al*. HDAC2 negatively regulates memory formation and synaptic plasticity. *Nature* 2009; **459**: 55–60.
- 60 Hanson JE, La H, Plise E, Chen YH, Ding X, Hanania T *et al*. SAHA enhances synaptic function and plasticity *in vitro* but has limited brain availability *in vivo* and does not impact cognition. *PLoS One* 2013; **8**: e69964.

Supplementary Information accompanies the paper on the *Molecular Psychiatry* website (<http://www.nature.com/mp>)